Chem Soc Rev

TUTORIAL REVIEW

Understanding the reactivity of metallic nanoparticles: beyond the extended surface model for catalysis

Francesc Viñes,[a] José R. B. Gomes[b] and Francesc Illas*[a]

Cite this: DOI: 10.1039/c3cs60421g

Received 19th November 2013

DOI: 10.1039/c3cs60421g

www.rsc.org/csr

Metallic nanoparticles (NPs) constitute a new class of chemical objects which are used in different fields as diverse as plasmonics, optics, catalysis, or biochemistry. The atomic structure of the NP and its size usually determine the chemical reactivity but this is often masked by the presence of capping agents, solvents, or supports. The knowledge of the structure and reactivity of isolated NPs is a requirement when aiming at designing NPs with a well-defined chemistry. Theoretical models together with efficient computational chemistry algorithms and parallel computer codes offer the opportunity to explore the chemistry of these interesting objects and to understand the effects of parameters such as size, shape and composition allowing one to derive some general trends.

Key learning points
- Understand the intimate chemistry of metallic nanoparticles.
- Approaches to model adsorption and catalysis at nanoparticles.
- Role of atomic coordination in adsorption and reactivity.
- Convergence to bulk material: scalable and non-scalable regimes.
- Quality of the calculations, computational limits, and interpretation of experimental data.

Introduction

Metallic nanoparticles (NPs) are ubiquitous in many areas of science, from physics to chemistry, materials science, and nanotechnology. From the point of view of fundamental physics, metallic NPs provide models to explore the effects of quantum confinement on optical, electronic, magnetic, and related properties.[1] The interest in the chemistry of metallic NPs is related to the effect of size and shape on their reactivity. The technologies related to these particles have a direct impact on society and industry since, for instance, they are key components of supported heterogeneous catalysts[2] working in environments as different as car exhausts, reactors in oil refineries, or in advanced photocatalytic processes.[3] In the past few years, metallic NPs have received increased attention because nanotechnology has opened the door to the synthesis of metallic NPs with controlled size and shape,[4] and because of the emerging applications in photonics, sensing, imaging, and even in medicine.[5] In particular, the study of the chemical and physical properties of solely Au NPs has become a blooming research field in itself with hundreds of articles published in the past few years.[6] Here it is worth pointing out that the literature on the field, especially regarding experiments and applications, is extremely immense, and the references provided are aimed to guide the reader by providing appropriate initial steps.

Understanding the intimate chemistry of metallic NPs is not a simple task since several factors are into play, such as the above-commented size and shape, but also the composition.[7] These have to be taken into account and, ideally, decoupled. In catalysis, metallic NPs are usually deposited onto a support, most often an oxide or a sulfide.[2] These systems are rather complex and experimental models have been proposed to control some of the parameters defining a supported catalyst by means of surface science techniques (ref. 8 and references therein). Nevertheless, the chemistry of metallic clusters in a homogeneous phase has also been the object of considerable attention since it is under these conditions that size and shape

[a] Departament de Química Física & Institut de Química Teòrica i Computacional (IQTCUB), Universitat de Barcelona, C/Martí i Franquès 1, 08028 Barcelona, Spain
[b] CICECO, Department of Chemistry, University of Aveiro, Campus Universitário de Santiago, 3810-193 Aveiro, Portugal

control is more easily achievable.[9,10] However, it is important to realize that, except in the case of gas phase clusters consisting of only up to a few tens of atoms,[11] metallic particles in a homogeneous phase are neither isolated nor clean, *i.e.*, they are commonly found in colloidal form and stabilized by solvent molecules, polymers, microemulsions, sol–gel, or clays.[9] The presence of the solvent and of the stabilizing agents renders the structural determination cumbersome.

Interestingly, back in 1995 it was possible to resolve the structure of Pd NPs of different sizes stabilized in solution in the presence of tetraalkylammonium salts by a combination of scanning tunnelling microscopy (STM) and high-resolution transmission electron microscopy (HRTEM).[12] Progress in the experimental characterization of metallic NPs has been made in the case of Pt, where model NPs were synthesized by lithography techniques and colloid chemistry.[13] These synthetic methods led to the formation of two-dimensional polymer-capped metal NP arrays, which can be characterized using various typical surface science techniques, such as X-ray photoelectron spectroscopy (XPS) and atomic force microscopy (AFM), either before or after chemical reactions take place. Precisely because of the presence of the capping agents, the application of STM to NPs thus obtained faces some not yet resolved issues.[14] The experimental technology reached a point where metallic NPs can be readily synthesized and characterized even at the subnanometre scale.[15] The use of wet chemistry approaches has also contributed to our understanding of heterogeneous catalysis. For instance, Turner *et al.*[16] were able to prepare Au/SiO_2 catalysts where the Au NPs were derived from 55-atom clusters (Au_{55}) and to study the selective oxidation of styrene with dioxygen without the presence of any oxidation initiator. However, even in such a controlled study, Q6 a distribution of Au NPs was obtained, which prevented the assignment of the observed reactivity to a particular type of NPs with well-defined size. Clearly, several challenges still exist concerning the intrinsic effect of size and shape on the chemical reactivity of metallic NPs. Again, the presence of capping agents and/or supports introduces additional complexity that renders the analysis of the chemical reactivity and potential catalytic activity a complicated task.

The tremendous progress in the synthesis of metallic NPs with controlled size and shape briefly outlined above does not yet permit one to obtain isolated and clean samples, clearly limiting our capability to understand all the occurring critical phenomena, a necessary step towards engineering NPs *à la carte* for a given application. Computational modelling offers a useful and complementary approach to experiments since dealing with isolated, clean, metallic NPs does not represent a problem, except for the computational resources, which become significant for quantum mechanical calculations concerning particles in the 1–10 nanometre range, easily involving hundreds to thousands of atoms. Still, approximate theoretical models have been designed for these large particles, which are based on classical interatomic potentials containing parameters fitted either to experimental material properties or to density functional calculations.[17] Nevertheless, modern computational codes and parallel computers can make these otherwise unfeasible calculations possible. In fact, significant progress has been made in the field regarding the structural properties of metallic and bimetallic NPs,[18] especially regarding the search for global minima in the smallest ones and tackling the problem of a multitude of isomers in medium and large size particles,[17] which becomes very relevant in the case of bimetallic nanoalloys. Here it is worth mentioning that the composition of the nanoalloy introduces an additional degree of freedom which may be used to engineer the reactivity of these nanoparticles towards a given direction. The presence of different types of metal atoms also introduces new types of active sites with a concomitant increase of complexity in the theoretical studies.

The progress in modelling metallic NPs with density functional methods has grown considerably in the last decade, after several important contributions which go well beyond the study of small gas phase clusters with only a few atoms. It is worth mentioning the strategy followed by Yudanov *et al.*[19] which consists of using moderately large NPs to simultaneously represent terrace sites of extended surfaces and low coordinated sites. In this way, it is possible to explore the chemistry of well-defined single crystal surfaces and of supported catalysis within the same model, a strategy which represents a leap forward with respect to models representing low coordinated sites by extended stepped surfaces.[20] For instance, with this alternative strategy, it is possible to gather information about the role of the particle size and to define the so-called scalable regime, as well as to study convergence of relevant properties towards the bulk.[21] The two concepts are related but different; the scalable regime is reached when properties such as interatomic distances or cohesive energy start to exhibit a linear trend with increasing number of atoms in the NP. This is opposite to the behaviour commonly found in small NPs, where non-monotonic trends are observed upon increasing the nuclearity: in this regime every single atom counts. Note, however, that in the scalable regime certain properties may vary so little with respect to the particle size that, for practical purposes, one may consider the value to have converged.

This is precisely the case for the calculated adsorption energy of a particular adsorbate on a given type of facet, or the development of the metallic electronic structure, eventually converging to the bulk. These are two crucial aspects determining the reactivity of metallic NPs. Clearly, establishing the scalable regime is important since it allows one to extrapolate properties towards larger NPs and to the bulk. On the one side Yudanov *et al.*[19] have shown that the calculated adsorption energy of CO on (111) terrace sites of truncated octahedral Pd NPs is converged for particles having about 80 atoms or more, exactly the same size at which Viñes *et al.* found the development of a characteristic metallic electronic structure close to that of Pd bulk.[22] Scalability and convergence become especially important regarding the chemical reactivity of the metallic NPs, with obvious implications for catalysis, because otherwise extracting general rules governing such processes in a systematic way becomes impossible.

The main focus of the present review is precisely on the chemical reactivity of metallic NPs with the aim of understanding the chemistry beyond these fascinating systems and, whenever possible, to provide a first step towards determining rules allowing making reliable predictions on the reactivity of unsupported particles. This constitutes a necessary gateway before attempting a rational, engineered modification of the reactivity of NPs. Improvements over the catalytic performance of metallic catalysts are induced, for instance, by an active interplay between the particle and support, as recently shown for the case of the water gas shift reaction by Pt NPs in $Pt/CeO_2(111)$ and $Pt/CeO_x/TiO_2(110)$ catalysts[23] or by nanoalloying, taking advantage of bimetallic catalysts but at the nanoscale.[18] The main hypothesis here is that a deeper understanding of the particularities of the chemistry of metallic NPs will allow improving their catalytic properties.

Building nanoparticle structural models

Because nanotechnology has emerged as one of the most important fields in physics, chemistry, and life sciences, the term NP is used in a very broad and often misleading way. In fact, nowadays the term NP is used in such a way that it covers almost all possible ranges from small gas phase clusters to very large particles containing thousands of atoms, including also cluster models representing extended surfaces. Fig. 1 displays a Pt_8 cluster, a three layer Pt_{29} cluster model representation of Pt(100), and a Pt_{598} cubo-octahedral particle with (111) and (100) facets, and illustrates these three quite well-defined regimes. The above words of caution apply not only to metallic NPs but to NPs in the most general sense.[24] Therefore a brief description of the different contexts is necessary to avoid misunderstandings and to be able to better focus the goal of the present review.

Small clusters, such as that depicted in Fig. 1a, have been extensively studied at both the experimental and theoretical levels,[25] Au clusters being probably the most representative because of their now well established, but once completely unexpected, catalytic properties.[26] Experimental techniques such as seeded supersonic nozzle techniques, gas aggregation, or laser vaporization, among others, are used as cluster sources.

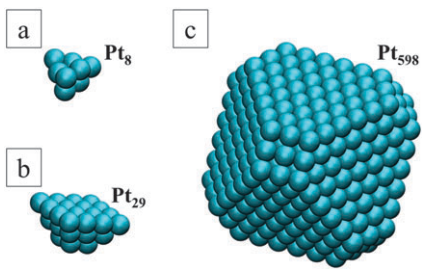

Fig. 1 Schematic representation of (a) a Pt_8 gas phase cluster, (b) a three layer Pt_{29} cluster model representation of Pt(100), and (c) a Pt_{598} cubo-octahedral nanoparticle exhibiting (111) and (100) facets.

The cohesive energy, or binding energy per atom, strongly oscillates with the number of atoms, and the same occurs with other physical and chemical properties,[17,25] arising from the relevance of geometric and electronic structure effects in the subnanometre regime.[26] Several features of the electronic structure as well as some other properties of these systems, especially for simple metals, are quite well understood, the so-called shell model providing quite a unifying picture. Nevertheless, it is important to point out that the success of this simple model is a consequence of the boundary conditions of the nearly free electrons in small particles of simple metal clusters.[25] Clearly, this simple model cannot account for the large variety of low lying isomers existing in a narrow energy range, which typically exhibit atomic structures hardly comparable to that of the bulk metal. The electronic structure of transition metal small clusters is a more complicated issue.[17] Moreover, the chemistry of small metal clusters is by no means simple; the adsorption energies of probe molecules such as CO or NO strongly oscillate with cluster size. These systems are representative of the non-scalable regime defined in the previous subsection, and should not be referred to as NPs but rather as metal clusters. Consequently, this type of systems will not be lengthily discussed here and for more exhaustive information the reader is referred to excellent reviews on the field.[17,18,25]

For completeness, it is worth mentioning that metal clusters containing a limited number of atoms have been broadly employed as surface models, especially in the 15 years spanning the 1980–1995 period.[27] In this approach, the structure of the cluster is cut from the bulk and usually maintained fixed with the crystallographic parameters taken from experiment (Fig. 1b). This choice, especially for small clusters, results in significant edge effects which, in turn, lead to a slow convergence of calculated results with respect to the cluster size. Precisely because of the edge effects, surface cluster models have been almost abandoned and substituted by periodic approaches, even if clusters have been very useful to unravel physical mechanisms related to local properties of adsorbate–surface interactions. The use of periodic surface models has been boosted by the appearance of quite accurate density functional theory based methods (see next section) and their implementation in efficient codes fully exploiting the translational symmetry. Cluster models of extended metallic surfaces may offer some advantages over the usual periodic slab model approach which, as already commented, has become the standard model in the theoretical study of surface chemistry and of the mechanisms of heterogeneously catalysed reactions. For instance, cluster models allow one to employ explicitly correlated wave function based methods which, when necessary, can be used to check the performance of a given density functional theory based method. Clearly, surface cluster models can be regarded as metallic NPs, but the choice of a particular cluster shape strongly determines their physical and chemical properties.

We come now to the type of metallic particles which can be effectively denoted as NPs; Fig. 1c provides a prototypical

example. These may contain from a few tens to several thousand of atoms, have dimensions within 1–100 nm and usually exhibit very well defined crystal facets. Precisely because of this particular feature, it is common practice to build NP models using the well-known Wulff construction, which was proposed as early as 1901. The physical basis behind the Wulff construction is quite simple and follows from the fact that the equilibrium shape of a crystal is necessarily that minimising the total surface Gibbs energy. The NPs built following this simple approach constitute a first approximate structural model, which can be refined in subsequent steps by energy minimization, using an appropriate method to estimate the total energy of the particle, as will be briefly discussed in the next section.

The Wulff construction may be viewed as a top-down approach since it starts from the knowledge of the surface energy $\gamma(hkl)$ of the exposed facets, which normally depend on the type of particle to be modelled. Usually one wishes to represent NPs exhibiting most stable surfaces but, depending on the type of study, it may be convenient to include more reactive surfaces. For a given application, a good strategy is to mimic the type of NPs which are revealed by TEM, a technique that permits one to obtain structural information of supported NPs even under realistic working conditions.[28] Once the morphology of the NPs of interest is defined, one needs to compute the set of surface energy $\gamma(hkl)$ values. This is a simple, standard, and almost routine calculation when employing appropriate slab models. Since the total Gibbs energy of a surface is given by the product of the surface energy γ and the surface area A, one can assume that the equilibrium structure of a NP with exposed facets with Miller indexes $\{hkl\}$ is such that

$$\int \gamma(hkl)\mathrm{d}A(hkl) = \text{minimum} \qquad (1)$$

where the integral involves all exposed facets; equation (1) is often referred to as the Wulff theorem. Wulff also proved that if $\gamma(hkl)$ is the surface energy of one of the exposed facets with these Miller indexes and $h(hkl)$ is the perpendicular distance from the surface to a point in the crystal known as Wulff's point, then for each of the exposed facets, the $\gamma(hkl)/h(hkl)$ ratio is constant. This allows one to construct the approximate equilibrium shape of the crystal following a simple recipe. The procedure, illustrated in Fig. 2, starts from an arbitrary point of the perfect crystal and draws vectors normal to the crystallographic planes of interest. Next, from an arbitrary $\gamma(hkl)/h(hkl)$ ratio, mark the distances $h(hkl)$ to each of the exposed $\{hkl\}$ surfaces along each of the vectors normal to (hkl) drawn in the previous step. The desired NP equilibrium shape is now simply obtained by adding planes perpendicular to the vectors through the marked points and taking the intersection of the planes. A more detailed description can be found in the excellent book by Desjonqueres and Spanjaard about surface physics.[29] It is also important to point out that more elaborate theoretical methods have been proposed to improve the original Wulff construction for isolated NPs. The approach designed by Barnard and Zapol[30] includes edge and corner energies, surface tensions, the bulk elastic energy and, in principle, can take into account experimentally relevant conditions such as surface composition or temperature.

The Wulff construction allows one to construct NP models with tailored facets, which can be used to study surface reactivity. Nevertheless, this constitutes only a starting point, and the final structure needs to be obtained by more elaborate first principles calculations as described in the next section. We must warn that the required calculations may be computationally very expensive or even unfeasible. Here it is where the concept of scalability defined in the introduction becomes tremendously useful. For very large NPs it may well be that structural, physical, and chemical properties can be predicted from the values computed for smaller but morphologically similar NPs. This is possible when the smaller NPs are already in the scalable regime, *i.e.* range of particle sizes where the properties of interest converge linearly to those of the bulk material as schematically illustrated in Fig. 3. Nevertheless, one must warn that not all properties will enter the scalable regime at the same size and, therefore, finding the onset for this regime and checking that it is fulfilled for the property under scrutiny is crucial. The concept of scalable regime is fundamental for modelling purposes since it allows one to estimate

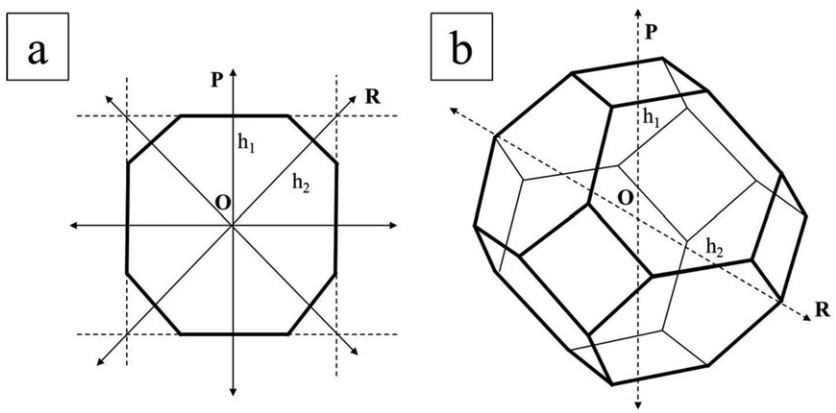

Fig. 2 Schematic representation of the Wulff construction for (a) a two dimensional case and (b) a three dimensional particle.

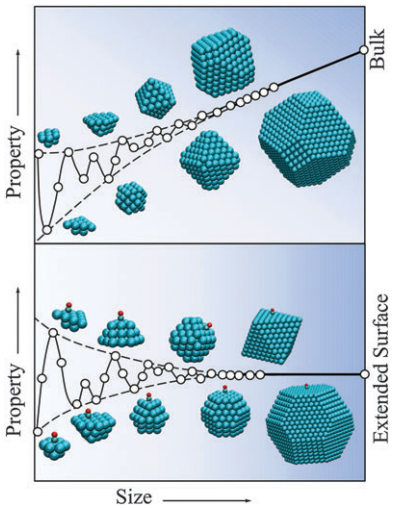

Fig. 3 Variation of an arbitrary property with the nanoparticle size either towards the bulk (top panel) or towards the extended surface limit (bottom panel), illustrating the scalable and non-scalable regimes.

properties of very large NPs from appropriate smaller equivalent ones.

Computational methods for metallic nanoparticles and their chemical reactivity

The interest in metallic NPs and clusters triggered several approaches, which are particularly well suited to explain experimental observations, such as the abundance and distribution of alkali clusters in the gas phase. The most popular method is based in the so-called shell model where a cluster is represented as a super-atom, with electrons fully delocalized in the cluster volume filling discrete energy levels. There are several implementations of increasing accuracy for this model. In the simplest one, the electronic structure is represented by a spherical Jellium model, which is similar to that used by Kohn and Lang in their seminal work leading to the interpretation of the surface work function in terms of a surface dipole (see for instance ref. 29 and references therein). The spherical Jellium model also assumes that the electron density moves in a uniform background of opposite positive charge but, in addition, includes an external potential. There are several forms of the potential, the simplest ones being the infinitely deep spherical and the harmonic well. The one electron Schrödinger equation for these simple models can be analytically solved and provide a series of levels, which allow one to understand the series of magic numbers observed in the experiments. Note, however, that this simple model hampers the study of bond breaking and bond forming at the metallic NP surface. Therefore, a more detailed description of the shell model and other more or less empirical methods based on the use of some sort of predefined potentials is out of the scope of the present work, and the reader is referred to some of the excellent reviews on the subject.[17,18] Note that methods based on such simplified forms of the interaction potentials acting on the particle atoms, such as molecular dynamics or Monte Carlo simulations, can be used to obtain important information about the structures of nanoparticles or about the surface segregation behaviours and phase stabilities of bimetallic nanoparticles for different ranges of alloy compositions, particle sizes, and temperatures. The main limitation of these approaches lies in the approximate nature of the interatomic potentials or force fields. Obviously, it is also possible to carry out molecular dynamics simulations at the *ab initio* level of theory, most often within a given DFT based method.[31] However, this implies that the forces acting on the atoms have to be computed (almost) every time step along the simulation which makes the approach computationally expensive, especially for studies involving large metallic nanoparticles with tens or hundreds of atoms. One must also realize that with the ever growing computational resources and the more and more efficient computational codes this type of studies will become routinely available and have the advantage of allowing one to study the temporal evolution of a given system at a given finite temperature. This may be important to understand changes in the reactivity of nanoparticles, either isolated or supported, involved in catalytic reactions under realistic conditions.

In order to study the reactivity of metallic NPs (or of any system) toward a specific reaction, it is necessary to explore the potential energy surface and to be able to characterize reactants, products, and transition states for the elementary steps of interest. This irremediably implies the use of quantum mechanical methods of electronic structure and also implies the need for considerable computational resources. Reactants and products are easily characterized by energy minimization followed by frequency analysis. However, the search of transition states associated to the elementary steps is often a worriment in theoretical reactivity studies. As will be described in the last section, transition state location *via* point-step or bond-constriction calculations appears to be simple and feasible; yet other techniques might be applied to gain non-trivial transition states, such as the climbing-image nudged-elastic-band (CI-NEB), which simultaneously optimizes intermediate structures along a reaction path, allowing the depiction of the reaction energy profile in which its highest point is the transition state. Alternatively, the Dimer method samples the potential energy surface by displacements of two interconnected structures; yet a good initial guess of the transition state is advised, and sometimes the Dimer method is used in combination with CI-NEB. In any case it is of outmost importance to characterize the structure located through these algorithms as a true transition state. To this end it is worth pointing out that a transition state structure must have a zero energy gradient vector (or with all components below a given threshold) and the energy Hessian matrix must have one and only one negative eigenvalue. These conditions are always taken into account in molecular chemistry studies but not always fulfilled in the surface science and catalysis literature.

The methods of electronic structure can be divided into two main families: in the first one, the goal is to find a suitable,

sufficiently accurate, approximation to the *N*-electron wave function, *N* being the total number of electrons in the system, whereas, in the second one, the aim is to extract the energy of the system and related properties from the electron density through an appropriate density functional; this is the basis of the so-called density functional theory (DFT) methods. An exhaustive description of the different methods of electronic structure requires several volumes and even a brief, schematic, explanation is out of the scope of the present review article and the interested reader is referred to the available excellent textbooks on quantum chemistry or on electronic structure. Here, it is enough to comment that wave function based methods become rapidly computationally too expensive with *N* to be useful to explore the electronic structure and reactivity of metallic NPs, whereas DFT based methods offer some hope and are nowadays the weapon of choice in this type of studies although these are not free of problems.

In order to understand the computational difficulties mentioned above it is sufficient to state that, even at the simplest Hartree–Fock level, where the *N*-electron wave function is represented by a single Slater determinant with orbitals usually expanded in a Gaussian type orbital (GTO) basis set and, hence, electron–electron interactions accounted for in an averaged way, the computational effort is unaffordable since the calculation of the necessary two-electron integrals typically implies a N^4 dependence of the computational time. The number of electrons explicitly treated can be reduced by including the effect of the core electrons in an effective core potential (ECP) or other similar approaches, usually referred to as pseudopotentials. The use of ECPs is now a routine in calculations involving heavy elements, and has the advantage of including scalar relativistic effects, which are mainly due to the high kinetic energy of core electrons. An additional problem with the Hartree–Fock method is that it lacks electron correlation effects arising from the instantaneous electron–electron interaction, which are crucial when bonds are broken or formed. The simplest way to include electron correlation effects is to take them into account by second order perturbation theory. The description of the system is improved but still faces problems when interatomic distances are elongated and, to make it worse, the computational effort scales as N^6. The computational burden increases if, in addition to the total energy, one needs to compute the energy gradients, a necessary requirement when aiming at finding optimum or transition state structures. Such structures have to be characterized, respectively, as minima or first-order saddle points in the potential energy surface, which requires additional frequency calculations. The latter calculations are unavoidable if the interest is on the chemical reactivity of NPs, the main focus of the present work. The use of linear scaling techniques and those based on the resolution of the identity allows one to carry out total energy calculations within these methods at a lower cost, but this is still excessive for a small NP, *i.e.*, a particle containing $\sim$100–200 atoms.

Density functional theory based methods also make use of a single Slater determinant but here to represent the electron density which, as in the Hartree–Fock methods, is given by a set of orbitals expanded in some sort of basis set. However, at variance of Hartree–Fock, in DFT based methods the total energy is not calculated as variational expectation value of the exact non-relativistic *N*-electron Hamiltonian but variationally extracted from an appropriate functional acting on the electron density, known as the exchange–correlation functional. Hohenberg and Kohn proved that such a functional exists although the exact form is not known. From the (unknown) exact functional one would obtain the ground-state exact energy and, hence, DFT based methods include electron correlation effects, the accuracy being provided by the choice of the functional. The simplest possible density functional is provided by the so-called local density approach (LDA), which assumes that the exchange–correlation potential depends on density only. Including the density gradient in a specific, well determined, form leads to the generalized gradient approach (GGA), a family of functionals including the broadly used Perdew–Wang (PW91) and Perdew–Burke–Ernzerhof (PBE) implementations. GGA functionals perform very well for metallic systems but are not as accurate for main chemistry elements. Mixing GGA exchange with non-local Fock exchange leads to the family of the so-called hybrid functionals, which are quite accurate for main chemistry elements. The interactions of adsorbates, normally containing main group elements, with simple or transition metals are usually well described with GGA functionals and, while accuracy is an unresolved issue, trends are usually correct. One current new way to remedy the DFT accuracy problem due to the neglect of dispersion terms is to include them either added to a standard exchange correlation functional as semiempirical interatomic dispersion potentials, or by the tuning up and adjustment of existing functionals to system datasets featuring diverse van der Waals interactions. Finally, it is worth pointing out that spin polarized density functional calculations can also be carried out when dealing with magnetic NPs or with open shell adsorbates. Nevertheless, the treatment of open shells is not a trivial issue and the reader is referred to more specialized literature (see ref. 32 and references therein). For more details on the basics of DFT based methods and their application to transition metal containing systems of interest in chemistry, the reader is referred to the recent review paper by Cramer and Truhlar.[33]

Because DFT based methods only require the electron density, the computational burden goes as N^3 and fully lineal schemes have also been proposed, which cannot be discussed here. This also implies a lower computational cost for energy gradients, geometry optimization, and transition state searches. Let us just add that the choice of the basis set needed to span the electron density is not a simple issue; GTO or Slater type orbitals (STO) are the normal choices although we will discuss below a convenient alternative. Nevertheless, DFT based calculations with GTO basis sets for quite large metallic NPs have been reported in the pioneering work of Yudanov *et al.*[19] These authors carried out DFT calculations for Pd NPs explicitly including all electrons and scalar relativistic effects. These calculations became possible because of the efficient and

smart use of point group symmetry, although this also implies the use of highly symmetrical models for the NPs of interest; for instance, octahedral particles were considered in ref. 19. It is important to realize, however, that while the use of symmetry allows one to study rather large isolated NPs, it becomes less efficient when considering the interaction of these particles with some adsorbate. One can still consider models where the presence of the adsorbate is replicated so as to keep the maximum symmetry. This strategy has also been followed by Yudanov *et al.*[19] by considering for instance the adsorption of CO at the top of the 6 vertices of metallic NPs with an octahedral shape. This is, no doubt, a valid and clever approach but it becomes hardly useful when the problem of interest concerns an elementary reaction at the NP surface, as will be shown below.

DFT based methods are very popular in solid state physics and surface science applications because of the relative facility to implement a periodic version of these methods, thus accounting for translational symmetry, which allows one to build realistic models of surfaces of solids. This is precisely the case when plane waves are used as basis sets to expand the electron density and it follows from the intrinsic periodicity of these functions. Plane waves describe the quantum state of a free particle in momentum space and a wave packet is necessary to avoid mathematical problems, as in the case of the well-known Dirac delta function, which also describes the quantum state of a free particle but in the position space. Therefore, one may intuitively argue that these functions are not appropriate to describe the state of electrons in bound states. Note, however, that because of the imposition of periodic boundary conditions, plane waves fulfil the requirements of quantum mechanics, and they are quadratically integrable and thus mathematically acceptable as basis functions; for a more elaborate discussion the reader is referred to the available textbooks in Quantum Mechanics. An appealing practical feature of plane wave basis sets is that the quality of the basis set, a delicate point and often a nightmare in quantum chemical calculations carried out with standard GTO or STO basis sets, is controlled by a single parameter, the kinetic energy cutoff controlling the number of plane waves in the calculations. In turn, the explicit description of the core electrons is difficult and requires an exceedingly large number of plane waves. Consequently, calculations with plane waves almost unavoidably use some sort of pseudopotential to represent the effect of the core electrons on the valence electron density. For a given accuracy, within a chosen density functional method, the number of plane waves is usually much larger than the number of GTO or STO basis functions but plane wave basis sets do not suffer from the well-known basis set superposition error characteristic of atom localized basis sets. The larger number of basis functions in the former case is not an issue since integrals involved are much faster when using plane waves. The latter offer also other additional computational advantages: the representation of the kinetic energy operator is diagonal, the energy derivatives are also computed in a faster way than when using localized basis sets, *e.g.* GTO or STO, and the overall procedure can be programmed in an efficient parallel fashion. Depending on the implementation, the number of iterations required to obtain a specific degree of accuracy becomes nearly independent of the system size. This is precisely the case of the widely used Vienna *ab initio* simulation package (VASP) for which an efficient implementation reaches a scaling which is almost linear with the number of atoms for systems containing up to 1000 electrons or more.[31] In the past few years, VASP has become a sort of standard in computational materials science although other schemes such as *PWSCF*, *Quantum Espresso*, *SIESTA* or *Ab Init* are available. At this point the reader may wonder about the relationship of these solid state methods and the subject of this work, *i.e.*, metallic NPs. The answer is very simple: within the periodic implementation of DFT based methods it is also possible to study finite, discrete, systems such as atoms or molecules – all that is required is to place the system of interest inside a sufficiently large box which is periodically repeated. For a large enough periodic box, the interaction between the artificially replicated images is negligible and this can be controlled by increasing the dimensions of the box until convergence is reached. Here it is important to note that the larger the periodic box the higher the kinetic energy cutoff for the plane wave expansion and the larger the number of plane waves to be included in the calculations. This is because of the need to fill the box space with a dense enough set of plane waves so that the electron density of the system can be accurately described.

The strategy outlined above has been tested by various authors on different types of metals including Fe, Pd, and Au (see ref. 22 and references therein). Here we will focus on the work of Viñes *et al.*[22] on a set of model Pd NPs exhibiting cubo-octahedral symmetry of increasing size. The resulting Pd_{38}, Pd_{44}, Pd_{55}, Pd_{79}, Pd_{85}, Pd_{116}, Pd_{140}, Pd_{146}, and Pd_{225} NPs include those used in the benchmark scalar relativistic DF calculations of Yudanov *et al.*[19] and, hence, allowed Viñes *et al.* to establish the accuracy of the plane wave periodic approach. These authors used the average coordination number N_{av}, defined as the sum of the coordination numbers of all n atoms of a cluster divided by n, and the fraction of surface atoms n_s/n to characterize the surface/bulk features of these Pd NPs, and have shown that these two parameters clearly exhibit the development of bulk character with increasing n. Interestingly, the calculated values for these two parameters also reveal that a particle as large as Pd_{225} is still quite far from the bulk limit. Fig. 4 reproduces the results of Viñes *et al.*[22] for the scaling of the average Pd–Pd bond distance d with the cluster size, and compares also with the all electron scalar relativistic calculations of Yudanov *et al.*,[19] which fully exploited point group symmetry. The emergence of the scalable regime is clear from the fitted correlation $d = 253.6 + 1.661N_{av}$ (in pm) which gives an extrapolated value for Pd bulk of 273.5 pm, very close to the 272.7 pm calculated value for bulk using the same density functional approach. Fig. 4 also shows that the values obtained from the plane wave periodic approach are in very good agreement with the results of scalar relativistic cluster calculations performed using O_h point-group symmetry, for

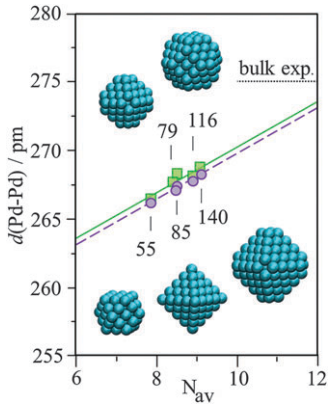

Fig. 4 Variation of the average nearest distances d(Pd–Pd) of Pd nanoparticles with the average coordination number N_{av}. The solid line corresponds to the plane-wave calculations of Viñes *et al.*,[22] whereas the dashed line corresponds to the all electron scalar relativistic cluster calculations of Yudanov *et al.*[19] Adapted with permission from F. Viñes, F. Illas, K. M. Neyman, *J. Phys. Chem. A*, 2008, **112**, 8911–8915. Copyright (2008) American Chemical Society.

which the fitted correlation was $d = 253.1 + 1.667N_{av}$ and the distance extrapolated to Pd bulk was 273.1 pm.[19] The average cohesive energy per atom is another important property providing information about convergence with respect to bulk and whether the scalable regime has been reached or not. Usually, this property is represented as a function of the inverse of the mean particle radius approximated by $n^{-1/3}$.[19] The results of Viñes *et al.*[22] using the plane wave periodic approach are perfectly linear. The extrapolation to bulk Pd agrees quantitatively with the corresponding bulk values calculated explicitly. A final aspect to be considered is the electronic structure of these Pd NPs and how the bulk-like electronic properties are developed for metal NPs of increasing size. The results of Viñes *et al.*[22] evidence a relatively fast evolution of the density of states (DOS) towards the bulk Pd with increasing particle size (see Fig. 5); for particles larger than Pd_{79}, the centre of the d-band, which is an excellent reactivity descriptor, approaches the bulk value.

Before closing this section it is important to comment on the electronic ground state of metallic NPs with or without adsorbates. For nonmagnetic metals, the electronic ground state is often of closed shell type and it is possible to use a single Slater determinant to represent the electron density. However, one must warn that small clusters on nonmagnetic metals may exhibit an open shell ground state and one must carefully explore different electronic configurations to ensure that the electronic ground state has been determined. The spin polarized version of DFT has to be used and one must be aware that the final density may not correspond to that of a state with well-defined multiplicity. It is even possible that the final electron density corresponds to a non-well defined mixing of different electronic states. This is indeed the usual situation when aiming at finding the electronic state of magnetic NPs. Note also that the presence of adsorbates, with or without open shells, can further complicate the situation since it may well be that the presence of the adsorbate changes the electronic ground state of the metallic NP. Note in passing that normally in such types of studies one focuses on total energy profiles only. A more accurate description would require consideration of the free energy profile and this requires taking into account entropy contributions; these are generally small when dealing with quite large metallic nanoparticles but can be important for small clusters. Finally, note that support effects may also affect the electronic ground state of the supported particle, especially in the case of magnetic metals. In the forthcoming discussion we will be mainly concerned with closed shell systems, and appropriate caveats about this particular issue will be included when necessary.

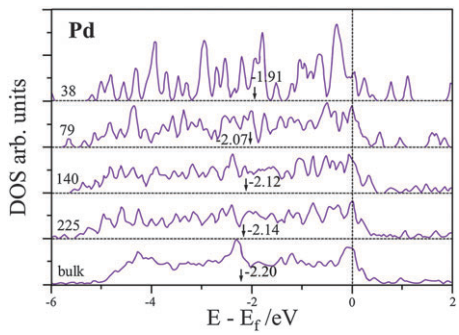

Fig. 5 GGA DOS plots for selected Pd_n NPs of increasing size (n = 38, 79, 140, 225) compared to the corresponding plot of bulk Pd. Arrows and numbers near them indicate centres of the d-band. Adapted with permission from F. Viñes, F. Illas, K. M. Neyman, *J. Phys. Chem. A*, 2008, **112**, 8911–8915. Copyright (2008) American Chemical Society.

To summarize, the electronic structure of metallic NPs of moderate size can be studied by the present state-of-the-art density functional theory based methods. Localized or plane wave basis sets can be used to accurately describe the main features of these particles. Selected results suggest that particles containing 100–200 atoms exhibit properties which are significantly different from the bulk limit but also that beyond this size one can safely assume that the scalable regime has been reached and that, for larger NPs, properties of interest such as cohesive energy (or adsorption energy of a given adsorbate as will be discussed in the next section) can be safely extrapolated from the trends exhibited by smaller ones in this regime.

Adsorption at metallic particles

The reactivity of metallic NPs for a specific reaction is intrinsically dependent on their size and shape and, therefore, it is tunable. Adsorption has a crucial role in catalysis since it determines the binding strength and the location of reactants in the catalyst and how these diffuse and react on the surface until products eventually desorb. These chemical processes usually involve several steps through a variable number of transition states depending on the complexity of the reaction, *i.e.*, depending on the number of elementary steps. Note that in some cases, the adsorption process is accompanied by catalyst surface reconstruction or refaceting. This intricate surface

chemistry makes the experimental study of the adsorption process at metallic particles a difficult task. Hence, computational studies involving well-controlled conditions assume a pivotal role in this respect, despite the consideration of several approximations in order to make the calculations tractable.

As introduced above, Yudanov *et al.*[19] considered symmetric (octahedral and cubooctahedral) Pd NPs and CO as a probe molecule, to investigate size effects on several calculated adsorbate/NP energetic and geometric properties. They described the structure of the NPs either with a bulk-terminated geometry, where the Pd–Pd nearest–neighbour distances were fixed at the experimental value of Pd bulk, *i.e.*, 2.750 Å, or with a fully optimized geometry within selected symmetry constraints, where the geometry of Pd NPs, with sizes ranging from ~1.1 nm (Pd_{55}) to ~1.9 nm (Pd_{146}), Fig. 6, is determined by a small number of symmetry-nonequivalent atoms (*e.g.* nine atoms in the case of the largest particles studied). In order to maintain the O_h symmetry of the bare particles in the CO/NP calculations, a CO molecule was inserted at each (111) facet in the Pd NPs, which corresponds to a total of eight CO molecules per particle. The interaction of CO with 3-fold hollow sites at the centre of the (111) facets showed that with the exception of the smallest particle, *i.e.*, Pd_{55}, the calculations provided rather uniform interatomic distances, vibrational frequencies and adsorption energies for the remaining particles considered, *i.e.*, Pd_{79}, Pd_{85}, Pd_{116}, Pd_{140}, and Pd_{146} (Fig. 6). In the latter, the adsorption energies calculated at the GGA–Becke–Perdew (BP86) level of theory, including corrections for the basis set superposition error, were found to vary in a narrow interval (171 to 176 kJ mol^{-1}), the adsorbate to substrate distances were in the range 2.038 to 2.067 Å and the C–O vibrational mode varied between 1738 and 1755 cm^{-1}. The calculated data for the smallest particle were 149 kJ mol^{-1}, 2.017 Å and 1711 cm^{-1}, respectively. As can be understood from these results, properties with a local character, *e.g.* bond lengths and frequencies, are not very different in the former and in the latter particles, but the adsorption energy on Pd_{55} is significantly smaller than that reported for the other five NPs. This is due to the incomplete coordination featured by the three Pd atoms forming the hollow site in the case of Pd_{55}. Thus, Yudanov *et al.* concluded that significant NP size effects are already eliminated for particles composed by about 80 Pd atoms. In fact, from comparison of the interaction energies calculated for the largest Pd NPs with the adsorption energies at 3-fold hollow sites, but on the extended Pd(111) surface, quantitative agreement was obtained. This seems to be a general conclusion if the same lattice constant and the same exchange–correlation functional are used for calculations involving NPs with sizes >~100 atoms or involving extended surfaces. Interestingly, the consideration of two other GGA functionals, namely, PW91 and RPBE, resulted in geometric parameters similar to those calculated with the BP86 functional for the largest Pd particles, but in quite different interaction energies, *e.g.* ~176 kJ mol^{-1}, 188 kJ mol^{-1}, and 142 kJ mol^{-1} for BP86, PW91, and revised PBE (RPBE) approaches, respectively.

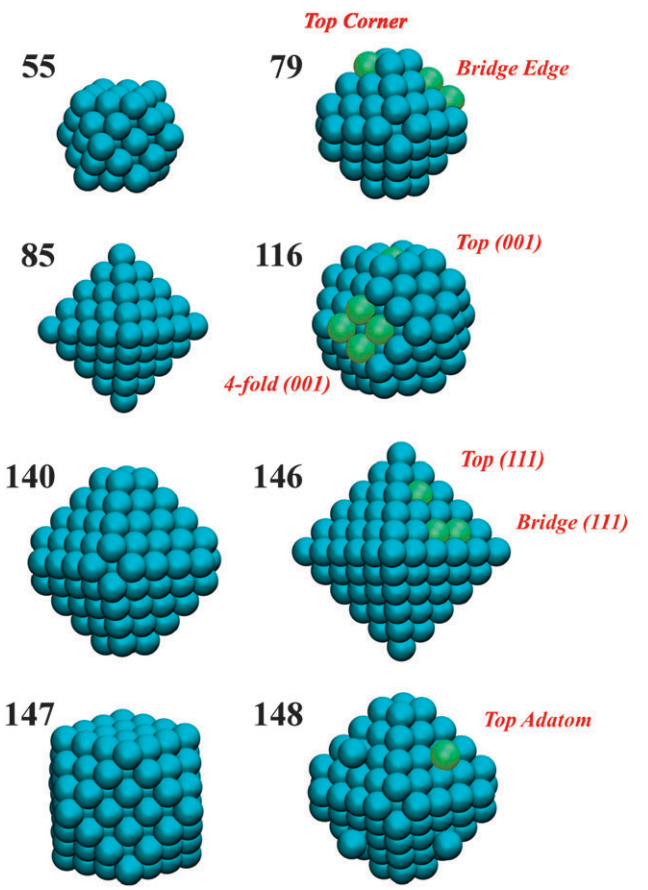

Fig. 6 Views of metal particles with O_h symmetry with nuclearities between 55 and 148. Adsorption site labelling (in red) is placed nearby the atoms they are conformed of, highlighted in light green. Adapted with permission from I. V. Yudanov, R. Sahnoun, K. M. Neyman, N. Rösch, J. Hoffmann, S. Schauermann, V. Johánek, H. Unterhalt, G. Rupprechter, J. Libuda, H.-J. Freund, *J. Phys. Chem. B*, 2003, **107**, 255–264. Copyright (2003) American Chemical Society.

Another important issue is the average metal–metal distance that is found to increase with the particle size. Yudanov *et al.*[19] found that the consideration of relaxed NPs (with Pd–Pd distances of ~2.69 Å or 2.65 Å, LDA approach, for the largest particles and for Pd_{55}, respectively) resulted in the reduction of the CO adsorption energies by ~10% (<20 kJ mol^{-1}) in the case of the larger clusters, while a more significant reduction, ~35 kJ mol^{-1}, was calculated for Pd_{55}. The reduction in the binding energies agrees with the principle of bond order conservation as a result of better saturated valences in the NP Pd atoms. The variation in the calculated C–O and adsorbate–NP bond lengths was quite small but note that adsorbate induced reconstruction of the Pd NPs was not considered.[19] The consideration of a GGA approach was found to yield Pd–Pd average distances that are ~0.1 Å longer. Thus, from what has been said above, the choice of the DFT functional has an evident influence on the values of the calculated adsorbate–NP energies; hence, it has a determining role in reactivity.

In a subsequent study, Yudanov *et al.*[34] extended their DFT calculations (BP86 approach and GTO basis sets) to the

interaction of CO with: bridge and top positions at the (111) facets; 4-fold hollow and top sites at (001) facets; bridge sites at particle edges; top sites at particle corners; and top sites above single Pd atoms deposited at the (111) facets using Pd NPs with 116, 140, 146, 147, and 148 Pd atoms (Fig. 6), in most cases with Pd–Pd distances fixed at 2.750 Å. In the case of the (111) and (001) facets, the relative strength of the adsorption positions found for the Pd(111) surface is maintained, *i.e.*, the interaction energy increases in the order top < bridge < hollow sites. In fact, Yudanov *et al.* found that if the atoms forming the adsorption site have coordination number nine, the calculated properties are very similar to those calculated on the ideal Pd(111) surface. Although the geometries are similar, the interaction of CO with positions formed by low coordinated atoms is much stronger. Actually, the binding energy at top sites on corners is ~30 kJ mol^{-1} larger than at top positions in the middle of the facets;[34] yet, the largest value for the interaction energy, 188 kJ mol^{-1}, was calculated for CO interacting with the bridge sites at the particle edges. The predicted effect of geometry relaxation on the energies calculated for CO interacting with low-coordinated atoms on large NPs was suggested to be ~10 kJ mol^{-1}, *i.e.*, similar to that found for high-coordination sites.

Based on the calculated energetic data, the experimentally observed vibrations at low pressure for CO adsorbed on bridge and top positions of Pd NPs containing approximately 400–3000 Pd atoms, deposited onto an alumina film, were assigned to adsorption on bridge sites at cluster edges and low-coordinated top positions, respectively. The experimental vibrations were obtained by infrared reflection absorption spectroscopy (IRAS) and sum frequency generation (SFG) techniques.[34] Despite the difference in the size of the Pd NPs studied computationally and experimentally, the calculated energetic data agree well with the observation of experimental vibrations for CO at the top positions on small, defect-rich, Pd particles at lower pressures than on larger, defect-poor, Pd particles. Similar conclusions were obtained by the same authors from another combined experimental and computational study where nitric oxide was selected as a probe molecule.

In a more recent work, Yudanov *et al.*[35] studied the size dependence of adsorption properties of metal NPs based also on DFT energies for CO interacting with Pd particles containing between 13 and 116 atoms, *i.e.*, they performed a detailed study on the non-scalable size regime for which deduction or extrapolation of properties is not possible. Note that particles with sizes in this region were suggested to be quite active for catalysis, so understanding how the reactivity of small metal particles scales with size is fundamental for the design of new catalysts. As expected, since small particles present atoms with a higher variety of coordination numbers, strong variations were calculated for the adsorption energies of CO on the particles with sizes below ~80 Pd atoms. Nevertheless, the variation of the largest adsorption energies on going from the smaller to the largest Pd NPs (Fig. 7) shows two opposite trends: in the scalable regime, the binding strength increases with the diameter of the NPs, which was suggested to be

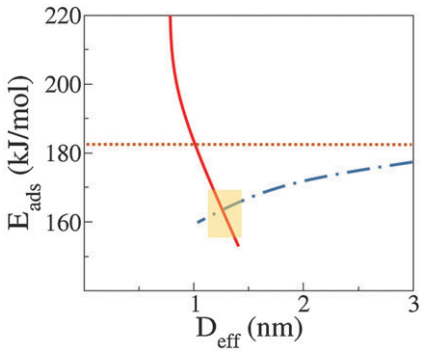

Fig. 7 Trends in the calculated adsorption energies (E_{ads}) for CO adsorption on Pd_n particles as a function of the effective particle diameter (D_{eff}). The yellow rectangle marks the critical size range, *i.e.*, particles with ~50 Pd atoms, where the dominant interaction mechanism changes from that associated with the non-scalable regime (solid line, E_{ads} decreases with D_{eff}) to the scalable regime (dot-dashed line, E_{ads} increases with D_{eff}). The dotted line represents the extrapolated E_{ads} for CO adsorption on an infinite Pd(111) surface. Adapted with permission from I. V. Yudanov, A. Genest, S. Schauermann, H.-J. Freund, N. Rösch, *Nano Lett.*, 2012, **12**, 2134–2139. Copyright (2012) American Chemical Society.

associated with an elongation of the average Pd–Pd distance caused by surface stress and a change in the van der Waals attraction (bonding competition); in the non-scalable regime, the binding strength decreases with the size of the NPs, which was associated to a shift of the centre of the *d*-band to larger binding energies with the increase of the particle size, in part as a consequence of a decreasing fraction of low coordinated atoms on the surface of the particle. The intersection of the two trends was found for particles with ~50 atoms for which the lowest energies for CO interacting with Pd NPs were calculated.[35]

The effects on the CO and O adsorption energies introduced by increasing NP size were recently investigated with DFT by Kleis *et al.*[36] using gold NPs with nuclearities 13, 55, 147, 309, 561, 923, and 1415 atoms and having diameters between 0.8 and 3.7 nm. The calculations were performed for fixed and relaxed geometries, the former with the adsorbate always at the same distance from the adsorption site in the different-sized particles to measure the electronic effects caused by varying the size of the particles. The general conclusion that the adsorption becomes stronger as the particle becomes smaller was still observed. The effects of relaxation in the adsorption energies for the smallest particles were found to be more important in the case of O than CO adsorption. In the case of CO, the energy variations were found to be similar to those reported by Yudanov *et al.* for the interaction with Pd NPs.[19] In other words, the calculations show that the electronic effects totally dominate the relaxation effects, *i.e.*, variations in the adsorption energies for frozen and relaxed calculations are smaller than those for different-sized clusters. Additionally, it is shown that even for the particle with 309 gold atoms, finite-size effects are still important, especially, in the case of O adsorption. Analyses of charge density difference plots between bare particles and particles interacting with an adsorbate show that the

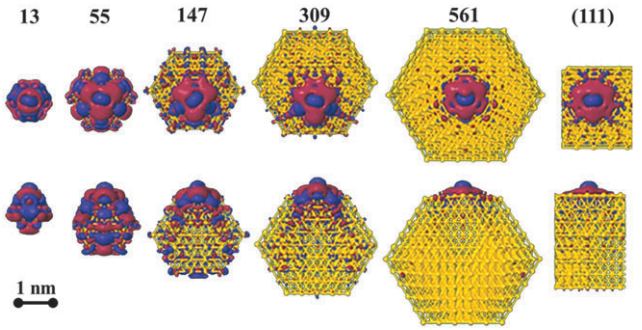

Fig. 8 Charge redistribution upon O adsorption on Au NPs seen from the top (upper row) and the side (lower row). Blue (red) contours signify areas of accumulated (depleted) electron density of ± 0.001 e Å^{-3} isocontour value. Adapted with permission from J. Kleis, J. Greeley, N. A. Romero, V. A. Morozov, H. Falsig, A. H. Larsen, J. Lu, J. J. Mortensen, M. Dułak, K. S. Thygesen, J. K. Nørskov, and K. W. Jacobsen, *Catal. Lett.*, 2011, **141**, 1067–1071. Copyright (2011) Springer Science + Business Media.

densities of gold atoms nearest–neighbouring and next nearest–neighbouring the adsorption sites are affected, *i.e.*, gold atoms at the edges are involved in the adsorbate–NP interaction, which suggests that convergence to Au(111) of the adsorption energies calculated for the particle with 309 gold atoms was not achieved (see Fig. 8). It should be noted that these effects are more evident for O than for CO adsorption, which is possibly due to the stronger binding of the former to metal surfaces.

The interaction of another strongly bonded adsorbate, atomic carbon, with either Pd or Pt NPs was reported in the literature.[37,38] These studies were inspired by the observation that adsorbed atomic C species are formed in the course of surface reactions. These species commonly decorate late transition metal (Pt, Pd, Ni, Rh, *etc.*) surfaces and constitute one of the major poisoning species of catalysts based on these metals, which are employed in a broad range of reactions dealing with organic molecules, *e.g.* steam and dry reforming and partial oxidation. The calculations performed with the PARAGAUSS code by Neyman *et al.*[37] were based on Pd particles with sizes ranging from $\sim$1.1 nm (Pd_{55}) to $\sim$1.9 nm (Pd_{146}) (Fig. 6), and show that C atoms are strongly adsorbed in the form of carbidic species that bear a significant negative charge. These authors found as well that the effect of spin polarization was quite marginal for the structure and energetics of bare and C covered palladium nanosize clusters. The changes in the cohesive energy and in the adsorption energy of C on threefold hollow sites of Pd_{85} are smaller than 1 kJ mol^{-1} when spin polarization is taken into account. The calculated data for the adsorption of carbon at the most abundant hollow sites in the middle of the (111) facets, for particles with Pd–Pd distances frozen at 2.75 Å, show adsorbate to particle heights of 1.86 ± 0.01 Å (LDA) and adsorption energies between 624 (Pd_{55}) and 657 (Pd_{116}) kJ mol^{-1} (BP86), or between 643 (Pd_{55}) and 677 (Pd_{116}) kJ mol^{-1} (PW91). Relaxation of all degrees of freedom but restrained to the intrinsic O_h symmetry of the models introduces small changes in the Pd–Pd and C–Pd distances and in the calculated adsorption energies. For instance, values of 2.70 Å, 1.86 Å, and 670 kJ mol^{-1} (BP86), respectively, were calculated for the Pd_{116} particle. Confirming conclusions from previous studies, convergence with particle size is faster for the distances than for the adsorption energies, and the relaxation contributions to the absolute values were found to be smaller than the effects introduced by different particle sizes. Interestingly, the calculations predict that the C atoms prefer to bind highly coordinated sites (hollow sites in the middle of the (111) or, preferentially, (100) facets), *i.e.*, an important destabilization was found for C located at sites near the edges of the (111) facets, which contrasts with the behaviour found for CO on Pd particles,[34] and with the results for the interaction of C atoms with Pt particles.[38] In the latter case, Viñes *et al.*, using the VASP code and the RPBE functional, found that the adsorption of carbon atoms seems to be enhanced near the particle edges.[38] Very recently, Aleksandrov *et al.*[39] performed another computational work analysing the interaction of C atoms with Pd NPs. In clear contrast with the results from the PARAGAUSS calculations of Neyman *et al.*,[37] the adsorption energies calculated with LDA, PW91, and RPBE approaches concerning the interaction of C species with sites near the facet edges are at least as favourable as with the hollow sites in the centre of the facets. This may be seen as another example of the important impact of the computational strategy on the calculated data for adsorbates interacting with metal particles.

Recently, some of us have been engaged in the computational study of the interaction of a single water molecule on a series of cubooctahedral Pt_n NPs of increasing sizes (n = 13, 19, 38, 55, 79, and 140).[40] Very interestingly, the calculations indicate that the adsorption energy of water is not significantly influenced by the NP size, with energies of 52, 45, 47, 57, 48, and 52 kJ mol^{-1}, respectively. These energies were calculated for water interacting with top sites at the particle edges (low-coordinated sites) and, not surprisingly, are considerably larger than the value of 26 kJ mol^{-1} calculated for water interacting with top sites on the extended Pt(111) surface. The quite converged interaction energies calculated for the water molecule on "computationally speaking" very small, small, and medium size Pt particles may be seen more as an exception than a rule. For instance, calculations with similar particles and computational parameters for O_2 on Au_n (n = 38, 55, 79, 116, and 147) NPs originated much larger energy differences, more precisely, adsorption energies of 93, 22, 27, 53, and 34 kJ mol^{-1}, respectively.[41]

Alloying assumes also a very important role in the structure and reactivity of bimetallic nanoparticles and this is quite an interesting topic since for the same structural nanoparticle skeleton it is possible to find different elemental arrangements. Despite the increasing degrees of freedom, computational studies are also currently used to understand the stability of binary nanoalloys and how adsorbates affect their chemical ordering. West *et al.*[42] used the PW91 approach to investigate the influence of CO and H adsorption on the chemical ordering of AB nanoparticles of the type AuPd, PdPt, CuPt and PdRh (and their inverses) with A_6B_{32} composition. They considered different elemental arrangements with 6 A atoms located in the core

or in the surface of the nanoparticles. A strong tendency to segregation inversion from AuPd shell–core to core–shell was found upon CO adsorption. Similar effects were observed for PdRh and PdPt but significantly less pronounced in the latter. Segregation inversion is due to the differential strength of CO binding which decreases in the order Rh > Pt > Pd > Au. In the case of CuPt nanoparticles, a strengthening of Pt–CO bonds was found when Cu neighbours surround the Pt atom interacting with the adsorbate; hence the Cu atoms migrate from the centres to the vertexes of the (111) facets in Pt-rich clusters. The effects caused by H adsorption were found to be qualitatively similar to those observed for CO but to a smaller degree to the point that segregation inversion is predicted for the AuPd pair only. Note that the calculations show that the segregation inversions observed for some systems are thermodynamically possible, which is in agreement with available experimental information, but information on the energy barriers is necessary to understand if these processes occur only under special experimental conditions and time scales.

Interestingly, properties of bimetallic nanoparticles do not always evolve linearly with composition. To understand these effects, Tang *et al.*[43] carried out DF calculations with the PW91 functional to estimate the binding energy of oxygen on hollow sites at the (111) facets of PdCu random alloy nanoparticles, with composition varying in 25% increments, and used the values as reactivity descriptors for the oxygen reduction reaction. They found that as Cu is added to Pd, the average binding energy is lowered until a minimum is found for 1 : 1 composition, which is quite intriguing since the binding to Cu is stronger than binding to Pd. Therefore, the synergy between the two metals is responsible for the unexpected trend. By decomposing the interaction of oxygen with the individual metal types, these authors found that charge transfer from Cu to Pd raises the d band of Cu and lowers that of Pd, resulting in a stronger binding of oxygen to Cu and weaker binding to Pd. The change in Pd is much larger than in Cu due to stronger overlap between the d-states of the metal and the adsorbed oxygen in the former than in the latter metal, which results in non-linearity of the oxygen binding energy and the Cu fraction in the alloy. More recently, An and Liu[44] used also the oxygen binding energy, calculated with the PW91 functional, to understand the size and shape effects of Pd@Pt core–shell nanoparticles (tetrahedron or sphere-like truncated octahedron) with nuclearities in the range 35–405 (1–3 nm) on the oxygen reduction reaction. They found that the binding energy with particle size varies differently on the sphere-like truncated octahedron and on the tetrahedron particles: A volcano-like relationship is observed in the former while an exponential-like decay is found in the latter. Such relationships seem to be well explained in terms of surface contraction in each type of nanoparticle considered by An and Liu.[44]

Reactivity on metallic particles

In this last section, a step forward is made going beyond the methodology suitability on metal NP adsorptive properties. The adequacy of the models and computational levels is proven by studying chemical reactivity on metallic NPs, simulating model catalysts composed of supported metal NPs on a given substrate, typically a metal oxide. Below we show, for selected exemplary reactions catalysed by metal NPs, how the reaction mechanism is not only dependent on the size and shape, but also intrinsically entangled to the availability of specific, low-coordinated sites, or the enhanced stability of reaction intermediates upon.

As already introduced the reagent adsorption has a key role in the catalytic process given that it is a necessary step. Moreover, the location and adsorption strength of reactants may bias the posterior reaction steps. Nevertheless, bond breaking–forming steps are the essential steps in the course of a catalysed reaction, and, consequently, the posed methodology must be suited to explore such steps in order to get information correlated with the experimental observations. One of the first paramount studies considering a catalytic process on metal NPs was that of Yudanov *et al.*,[45] who studied the C–O bond dissociation on Pd nanocrystallites in the course of methanol decomposition. The authors investigated not only the adsorption of a handful of species on a cubooctahedral Pd_{79} NP, including CH_xOH_y (x = 0–3, y = 0–1), but also CH_x (x = 0–3), OH, and O and C adatoms, but also the C–O bond scission of the adsorbed CH_xOH_y intermediates. The calculations, carried out with the PARAGAUSS code, took advantage of point-group symmetry, as already mentioned in various examples described in the previous section. Note, however, that in order to avoid artefacts and local restrictions, calculations were performed, when necessary, with symmetry reverted from O_h to D_{4h} or D_4, *i.e.*, revoking mirror planes. In this manner, the investigation of processes with adsorbates cross-edging neighbouring (111) facets is allowed. This restriction hinders the power of using point group symmetry, but infers versatility to the method. In any case, in order to alleviate the computational burden, ECP pseudopotentials were applied on the Pd core electrons. Calculations used also GTO basis sets and the BP86 functional. Transition states were located using a constrained optimization approach, where reaction paths were explored by fixing the C–O bond length and optimizing all other variables. The located transition states were characterized by a zero gradient and a Hessian matrix with only one negative eigenvalue.

Experimentally, it is found that methanol decomposition on Pd catalyst occurs with high selectivity toward CO/H_2. However, the overall activity is impeded by the catalyst modification by CH_x deposits, mostly carbonaceous species. The DFT calculations of Yudanov *et al.* permitted to depict a rather clear picture of the methanol decomposition (see Fig. 9), which provides an answer to the experimental observation, rendering a microscopic detail never gained before. Upon physisorption, the methanol molecule is prompted to lose one of the methyl hydrogen atoms. This dehydrogenation step was previously calculated to be exothermic by 45 kJ mol^{-1} on a Pd(111) slab model—VASP, PW91—with a small activation barrier of 33 kJ mol^{-1}. On the NP the exothermicity of this step is found to be slightly reduced to 25 kJ mol^{-1}, and a similar variation is

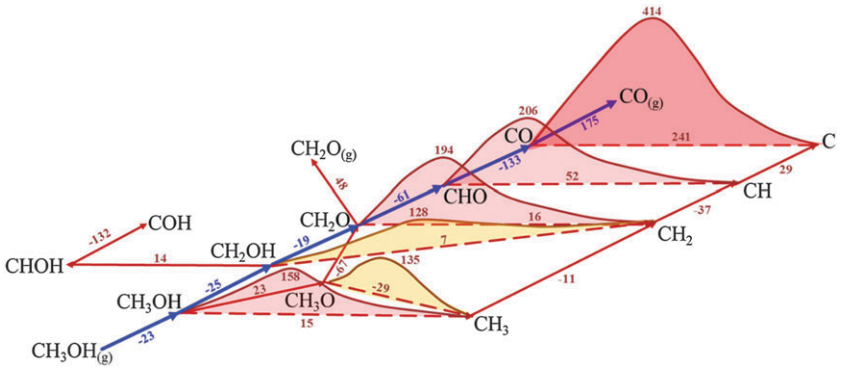

Fig. 9 Methanol and selected intermediates of its decomposition: reaction energies (kJ mol^{-1}) for the splitting of CH, OH, and CO bonds as well as for CH_3OH, CH_2O, and CO desorption as calculated on (111) facets of Pd_{79}. The main reaction path is highlighted in green, whereas CO dissociation barriers are denoted by orange lines and numbers. Adapted with permission from I. V. Yudanov, A. V. Matveev, K. M. Neyman, and N. Rösch, *J. Am. Chem. Soc.*, 2008, **130**, 9342–9352. Copyright (2008) American Chemical Society.

foreseen for the reaction step energy barrier. In subsequent steps the alcohol group of the CH_2OH intermediate is broken to form formaldehyde, CH_2O, and this latter molecule suffers consecutive dehydrogenations until forming CO. These last three steps were found to be exothermic by 19, 61, and 133 kJ mol^{-1}, respectively. Despite that the energy barriers of such dehydrogenation steps were not explicitly studied, it is worth mentioning that oftentimes the degree of endo/exothermicity of a reaction step influences the height of its reaction energy barrier, as explicitly commented below regarding Brønsted–Evans–Polanyi (BEP) relationships. This influence is clearly observed in Fig. 9 for C–O bond scissions: the larger the endothermicity of a reaction step, the higher the reaction energy barrier. In this sense, one would foresee dehydrogenation steps from CH_2OH to CO to feature relatively low energy barriers, and likewise for dehydrogenation steps from methyl groups to CH.

Concerning the carbon formation, it is unlikely to have originated from CO molecule dissociation in light of the calculations. This step is estimated to be highly endothermic (241 kJ mol^{-1}), and features an even higher activation barrier of 414 kJ mol^{-1}. Therefore, the C formation is more sensible to occur *via* the breaking of the C–O bond from any of the CH_xOH_y reaction intermediates. The calculations on the Pd NP models permitted to estimate that the lowest barriers for C–O scission are found for CH_3O and CH_2OH intermediates, with activation barriers of 135 and 128 kJ mol^{-1}, respectively, *i.e.*, few times lower than the barrier for the CO molecule. Note also that the C–O scission for CH_3O is an exothermic process by 29 kJ mol^{-1}, but CH_2OH C–O scission is essentially isoenergetic (endothermic by 7 kJ mol^{-1}, within the method accuracy). Note that despite CH_2OH is a reaction intermediate during CO formation, the C–O scission for CH_3O cannot be ruled out, since its formation from physisorbed methanol is endothermic by only 23 kJ mol^{-1}. In conclusion, the calculation on the Pd NP models led to the conclusion that carbonaceous formation is likely to proceed as a very slow by-process accompanying the dehydrogenation pathway, in particular, through the formation of CH_3O or CH_2OH intermediates and eventual C–O bond scission. Yudanov *et al.* also found that once CH_3 and CH_2 species are formed, the following dehydrogenation steps are estimated to be exothermic by 11 and 37 kJ mol^{-1}, respectively, whereas C adatom formation from CH is moderately endothermic (29 kJ mol^{-1}). All in all, the formation of carbonaceous species during methanol decomposition into CO/H_2 seems to be determined firstly by an easier C–O bond scission on CH_3O and CH_2OH intermediates, biased by the single (σ-type) C–O bond breaking, in juxtaposition to C–O scission from the CO molecule or other intermediates, which resulted in larger activation energy barriers due to strengthening of π-contribution to the C–O bond. Besides, the process is also equally influenced by the preferential occupation of CH_3 and CH_2 species at the edges of the Pd NPs, whose binding energies are 65 and 36 kJ mol^{-1} stronger than on the middle of the (111) facet, inherently prompting the C–O bond scission at these sites.

It is worth mentioning that a subsequent DFT theoretical work combining Pd(111) slab and Pd_{140} NP models showed that C adatoms are thermodynamically driven to occupy octahedral or tetrahedral subsurface sites.[46] On the Pd(111) surface, subsurface diffusion of C adatoms features distinctive activation energy barriers in the range of 50–60 kJ mol^{-1}, where subsurface octahedral sites are clearly preferred over subsurface tetrahedral sites. In contrast, on the Pd_{140} NP low-coordinated sites, such as edges and corners, a sensible stabilization of subsurface C is observed, by up to ~30 kJ mol^{-1}, when occupying subsurface tetrahedral sites, thus levelling its stability to vicinal octahedral sites. Moreover, while the subsurface diffusion energy barrier for C adatoms located at the centre of Pd_{140} (111) facets is similar to that obtained on Pd(111) slab, the barriers drop to a few kJ mol^{-1} or essentially vanish for sites nearby or located at edges and corners. The key role of low-coordinated sites in having subsurface C species was found to be intimately correlated with the enhanced fluxionality of metal atoms at these sites, which not only allows for a better accommodation of species upon or within, but here is also at the origin of the substantial subsurface diffusion activation energy reduction.

We now come back to the particular stabilization of CH_3 and CH_2 species at unsaturated sites, which was also detected in the

study of Viñes *et al.* concerning the methane activation by Pt NPs.[47] Here, CH_4 adsorption and its complete dehydrogenation were studied on a Pt_{79} NP at the RPBE level. In contrast to the previous study by Yudanov *et al.*,[45] who used a molecular code, the authors carried out the calculations with the VASP code, in which periodic conditions are imposed. This choice enabled one to get rid of point group symmetry constraints and to study the decomposition of a single molecule per particle, but also allowed direct comparison with extended slab calculations using the same basis set and calculation parameters. That was indeed the case for methane dissociation, where a split-and-win modelling strategy was applied to model Pd NPs of a few nm in size, in which slab calculations served to model the inner parts of facets, whereas the Pt_{79} NP permitted to simulate the catalytic activity of low-coordinated sites, such as edges and corners. Activation energy barriers for dehydrogenation steps were obtained by locating the transition states using the CI-NEB, and, as done in the work of Yudanov *et al.*,[45] they were characterized as so by a vibrational frequency analysis, a fact that allowed correcting the energy profiles with the zero point energy (ZPE) vibrations.

As already introduced, the intermediate species of methane dehydrogenation, namely, CH_3 and CH_2, were found to be stabilized, by 50–80 kJ mol^{-1}, at particle edges and corners. For other reaction species also such stabilization occurs, but to a lesser extent. This enhanced activity seems to stem out from two factors: low-coordinated sites are intrinsically more active to bind species upon due to their unsaturation. Besides, as found for the subsurface C on Pd NPs,[46] the metal atoms at these sites feature a natural larger flexibility to accommodate adsorbates. This, *a priori*, simple factor can be translated into substantial differences in both the thermodynamics and kinetics of the reaction. See, for instance, the reaction profiles displayed in Fig. 9 for the complete dehydrogenation of CH_4 on the Pt(111) surface and on the Pt_{79} NP. One of the main points is that methyl and methylene formation reaction steps are endothermic for single crystal surfaces, whereas they are clearly exothermic on Pt_{79}. This has a remarkable effect on the first methane C–H bond scission, which is normally the rate-limiting step due to the high CH_4 stability. The methane dehydrogenation barrier is ~60 kJ mol^{-1} reduced compared to the one on the Pt(111) surface. Furthermore, a similar reduction of ~40 kJ mol^{-1} is observed for methyl decomposition. Regardless of the substrate, or, in other words, the catalyst site, CH species seems to be the most likely end of the reaction. However, C adatom formation is found to be thermodynamically driven at particle edges and corners, although overcoming a high energy barrier of almost 100 kJ mol^{-1}. The computationally derived scenario fits perfectly with the single crystal and NP experiments. On single crystal surfaces, methyl species are found to be major species when dosing methane with a supersonic beam. Only after heating recombination of methyl species is observed, with the simultaneous desorption of CH_4 and formation of CH and C species. On NPs, X-ray photoelectron spectroscopy (XPS) measurements reveal a rapid formation of methyl species (at facets and edges), followed by the sequential formation of CH and C species (at edges and corner sites) at surface temperatures as low as 100 K, in concordance with the reduced energy barrier for methyl decomposition, as observed in Fig. 10.[47]

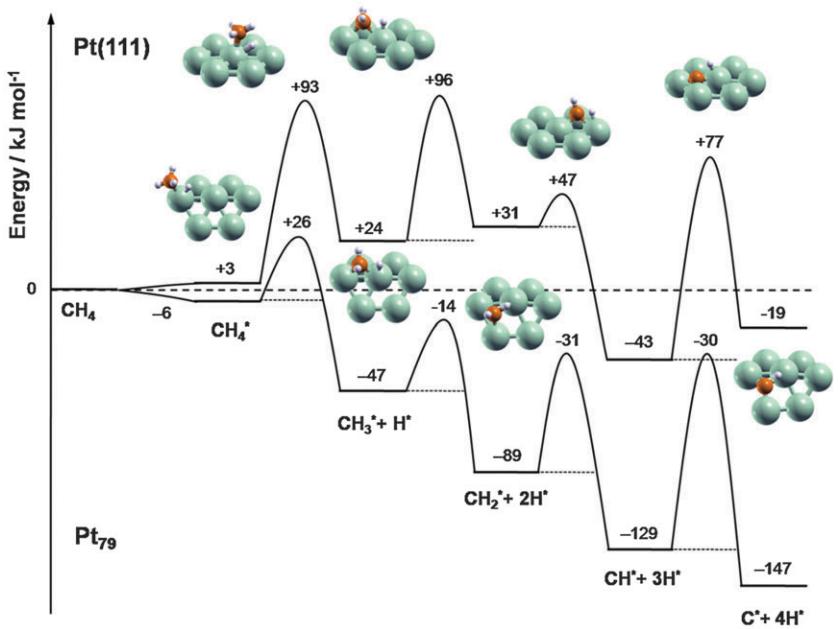

Fig. 10 ZPE-corrected reaction energy profile for the complete dehydrogenation of methane on a Pt(111) surface and on a Pt_{79} nanoparticle. All energies, in kJ mol^{-1}, refer to methane in the gas phase and the clean substrate. In the sketches of the transition states, only small portions containing seven Pt atoms of the calculated slab and cluster models are displayed for the sake of visual recognition. Adapted with permission from F. Viñes, Y. Lykhach, T. Staudt, M. P. A. Lorenz, C. Papp, H.-P. Steinrück, J. Libuda, K. M. Neyman, and A. Görling, *Chem.–Eur. J.*, 2010, **16**, 6530–6539. Copyright (2010) Wiley-VCH Verlag GmbH & Co.

One interesting point of this study is that the exothermicity increase of a reaction step—originated from an enhanced stability of the formed species—is accompanied by a reduction of the reaction step activation energy barriers. In this regard, BEP relationships linearly relating the activation energy for a given elementary step with its corresponding reaction energy can be summoned. This aspect was succinctly introduced in the work by Viñes *et al.*,[47] but fully investigated in a recent work by Fajín and co-workers on the water dissociation on Pt NPs,[40] studied as an elementary step of the steam reforming of methanol or methane carried out on Pt model catalysts. Fajín *et al.* studied the adsorption of a single water molecule and its homolytic dissociation on Pt_{13}, Pt_{19}, Pt_{38}, Pt_{55}, Pt_{79}, and Pt_{140} NPs, and compared the process to the extended Pt(111) slab situation, carrying out DFT calculations with the PW91 exchange–correlation functional. Similar to the above-commented methane dehydrogenation study, the authors took advantage of a periodic code, found transition states with the Dimer method, and identified them as so with a vibration analysis. Reaction profiles were ZPE-corrected. As a step further, reaction rate constant estimations were acquired from transition state theory, thus fully exploiting the theoretical machinery in the description of a catalysed reaction. In that work, the effect of spin-polarization was explicitly addressed, since it was found for small Pt clusters, such as Pt_8, that the optimal number of unpaired electrons had a direct impact on the cluster activity. However, for larger NPs either closed shell states were found or the spin-polarized solution was only minimally lower in energy, $\sim$0.1 kJ mol^{-1}, with a negligible effect on the cluster or NP catalytic activity. As commented in the previous section, the usage of smaller clusters or larger NPs led to small changes in the adsorption of H_2O, presumably due to the weak sorption of water (physisorbed state), which makes it structure/substrate-independent. This is not the case, though, for the estimated H_2O dissociation energy barriers: as shown in Fig. 11, the activation energy barriers sensibly oscillate for the smaller clusters, a clear reflection that such NPs are out of the scalable regime. However, the Pt_{140} barrier is of the same order of the Pt(111) limit, indicating that convergence with size is reached. In addition the authors found linear dependency of the activation energies with respect to the degree of exothermicity, *i.e.*, a BEP relationship, although the fitting was less quantitative than previous calculations exploring water splitting on the (111) surface of different transition metals. One particularly interesting point of such study is that H_2O dissociation is likely to occur since the dissociated species are energetically equal to or lower than adsorbed water, but also it is a requirement that the dissociation transition state lies lower in energy than the desorbed water situation. In other words, if the transition state corresponding to the reaction of H_2O dissociation lies above the energy level of a non-interacting system containing the water molecule and the Pt NP, then the adsorbed molecule is likely to desorb rather than decompose. However one must note that despite that the above reasoning is sensible, such standard DFT calculations did not account for a description of dispersive interactions, which can lower, to a certain extent, the energy of the interacting systems with respect to the non-interacting energy reference. Having this caveat in mind, the authors found that the larger the NP, the less favourable the water dissociation: optimum size is found for (sub)nanometre size clusters.

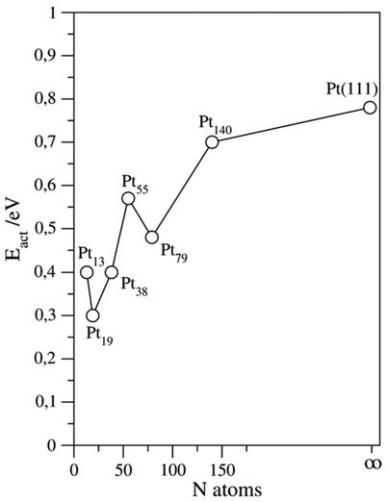

Fig. 11 Activation energy barrier with respect to the number of atoms in the Pt nanoparticles or extended (111) surface. Adapted with permission from J. L. C. Fajín, A. Bruix, M. N. D. S. Cordeiro, J. R. B. Gomes, and F. Illas, *J. Chem. Phys.*, 2012, **137**, 034701. Copyright (2012) American Institute of Physics.

The particular aspect above was the leitmotiv in the investigations of Roldán *et al.* concerning the O_2 dissociation on Au NPs (see ref. 41 and references therein), a work triggered by the effective catalysis of Au_{55} on the styrene selective oxidation,[16] or the low temperature oxidation of CO, as found by Haruta when supporting Au on TiO_2.[48] The authors explored the catalytic activity of a series of Au_n clusters (n = 5, 13, 25, 38, 55, 79, 116, and 147) by studying the O_2 adsorption and dissociation upon, using the *VASP* code and the PW91 exchange–correlation functional. Transition states were located by combining CI-NEB and Dimer methods, and they were confirmed as transitions states *via* a vibrational analysis. One of the most striking findings was that the O_2 dissociation activity was probably not due to the Au_{55} NP, as previously suggested, since for this particularly stable NP, O_2 desorption required significantly less energy (18 kJ mol^{-1}) than dissociation (energy barrier of 71 kJ mol^{-1}). Note that the difference between reaction and desorption energy is large enough so that the final picture would not be influenced even when accounting for dispersive forces. A similar situation was noticed for larger clusters, with adsorption energies in the range of 30–50 kJ mol^{-1} and O_2 dissociation activation energies in the range of 40–55 kJ mol^{-1}. Thus, energy barriers only slightly depend on the particle size, whereas a larger variation is found for adsorption energies. This was observed to be intimately related with the existence of a gap in between the occupied and unoccupied states of the pristine NP: when a gap exists, like in Au_{38}, it allows accommodating bonding states with O_2 below the Fermi level, resulting in a stronger interaction, while in the absence of a gap, *i.e.*,

metallic electronic structure, as happens for larger Au NPs, the interaction renders bonding and antibonding states, resulting in a weaker O_2 interaction. Thus, O_2 dissociation seems to be strongly governed by the O_2 adsorption strength, in contrast to H_2O dissociation on Pt NPs, where the activation energy barrier was governing the process. In fact, it is for the Au_{38} particle that the authors found an adsorption energy (88 kJ mol^{-1}) larger than the dissociation energy barrier (44 kJ mol^{-1}), suggesting that this—and other clusters of similar size—is well-suited for the O_2 dissociation catalysis. Thus, the experimental observation of the high activity of Au_{55} in O_2 dissociation may be apparent, and the activity is due to smaller clusters, given that in the experiments a distribution of Au NPs was obtained. Note that this situation however can change for very small clusters: for instance, the O_2 desorption and dissociation are both competitive situations on Au_{25}, whereas for smaller clusters, Au_5 and Au_{13}, the dissociation barriers are markedly higher, 271 and 279 kJ mol^{-1}, respectively, although adsorption energy is still calculated to be $\sim$50 kJ mol^{-1}. Moreover, the O_2 dissociation paths are found to be intimately ligated to the existence of (001) like facets, especially on the medium and large size NPs, highlighting the key role of the existence of such facets in the O_2 dissociation and, presumably, in the commented Au-catalysed reactions, a fact associated to the specific NP shape.

In order to mimic possible charge transfer effects arising from the presence of a support, the same authors investigated the effect on negative and positive charge on such Au NPs, *i.e.*, considered the charge effect on O_2 adsorption and dissociation. This is a simple but efficient way to emulate the possible slight reduction/oxidation of such gold NPs when supported onto an oxide substrate. Beyond the non-scalability region found for clusters below $\sim$80 atoms, already commented, the study unfolded that the addition of positive/negative charge has a significant effect on ultra-small clusters containing $<$20 atoms. In principle, the negative charge is beneficial in the sense that it lowers the O_2 dissociation energy barrier and stabilizes the final products. However, as mentioned, the barriers are quite high for such clusters, and the O_2 dissociation is unlikely because the molecule would rather desorb. The opposite trend is found when adding a positive charge to the Au NP, *i.e.*, removing one electron. Indeed such trends are found for any of the studied sizes, although the effect is rather mild for medium (Au_{38} and Au_{55}) and large NPs (Au_{79}). Curiously, the inclusion of charge does not ameliorate the catalytic activity on O_2 dissociation, that is, Au_{38} is active and the other particles are not, regardless of the charge state. Last but not least it was found that adsorption geometry, binding strength, barrier height, and product stability are mostly independent of the cluster charge state.

These previous studies triggered a theoretical work by Boronat and Corma,[49] where O_2 dissociation was investigated on the Au(001) surface, given the key role of such sites in the process, on the Au_{38} NP, given the suited catalytic activity reported, and on a hemispherical Au_{13} cluster unsupported or supported on a TiO_2 slab, in both cases containing the same active site as in the Au_{38} NP. DFT calculations were carried out using the VASP code and the PW91 exchange–correlation functional; transition states were obtained using the Dimer method, and characterized by the pertinent frequency analysis calculations. The results showed that O_2 dissociation on regular Au(001) surface is not viable, given that the activation barrier of 42 kJ mol^{-1} is larger than the O_2 desorption energy of 21 kJ mol^{-1}. Results on Au_{38} confirmed the previous findings of Roldán *et al.*,[41] whereas for unsupported Au_{13} the dissociation path in which O_2 is attached with a binding strength of 95 kJ mol^{-1} to a bridge–bridge site at the (001) facet leads to dissociation through a small energy barrier of 17 kJ mol^{-1}. In fact, the highest degree of molecular activation is always related to the existence of bridge–bridge conformers on (001) surfaces or facets. Additionally, the authors found, nevertheless, that the easiest path to dissociate O_2 on Au_{13} is when supported on TiO_2. In the latter, O_2 is preferentially adsorbed at the metal–support interface, *i.e.*, at the boundary region of the Au_{13} cluster, and thus in close contact with both the gold cluster and the titania substrate. The adsorption energy of 232 kJ mol^{-1} is accompanied by a moderately high dissociation energy barrier of 106 kJ mol^{-1}, highlighting the possible low-rate side process at boundary regions. In any case, such study must be taken with caution since it deals with a cluster out of the scalable regime, and thus the results should not be extrapolated to larger NPs, since this peculiar activity could be solely attributed to this particular particle. In any case the results tend to suggest a rapid O_2 dissociation on (001) facets of small Au clusters, and a slow by-process at the metal support interface.

Last but not least, it is worth mentioning the recent study of Cao *et al.*,[50] who studied N_2 dissociation on an Al_{44} cluster in both its cationic and anionic form, similar to the O_2 dissociation on Au NPs.[41] Here calculations accompanied experimental cross section chemisorption experiments, which found a kinetic energy threshold of 3 eV for solid particles and a drop to 2 eV for the melted clusters. The theoretical study combined static DFT PBE calculations using the SIESTA code, but also constant-energy *ab initio* molecular dynamics carried out at the same computational level, thermalizing the cluster at desired temperatures, and simulating the collision of a N_2 molecule with a given kinetic energy. Results revealed that N_2 dissociative adsorption is exothermic by $\sim$3 eV for both the anion and cation in the solid phase, but is reduced to $\sim$2.3 eV for the melted cluster, in good agreement with the estimated experimental value of 2.4 eV. Note that the exothermicity reduction does not lead to an increase in the reaction energy barrier, but the opposite: energy barriers were calculated to be 4 and 3.4 eV for the cation and anion in the solid phase, but reduced to 2.3 and 1.8 eV, respectively, for melted clusters. The highlight here is that the application of molecular dynamics enabled to show that the activation of a diatomic molecule on a metal nanoparticle may be sensibly favoured when accounting dynamic effects, opening a way for catalysis with liquid metals; yet application on larger particles in the scalable regime is still a milestone to be reached.

Concluding remarks and perspectives

The previous sections have illustrated how suitable models of metallic NPs can be built and how they can be used to extract general trends about their adsorptive properties and chemical reactivity towards several simple yet important reactions. The presented studies are selected research from the literature, chosen because they are representative enough, because they involve NPs of different sizes allowing one to derive trends and, finally, because they constitute clear examples where the potential energy surface has been explored and transition state structures determined. Clearly, for very large NPs, surface sites can be represented by suitable periodic slab models. This is not only the case for terrace sites but also for edge sites at the intercept of surfaces with different Miller indexes, which can be featured by stepped surface slab models as well although the size of the unit cell becomes large. However, these models, while valid and useful, miss the peculiarities that size and shape confer to the NPs mostly described in the present work, which allowed one to derive a few general rules.

The systems reviewed in the present work have also been deliberatively chosen as monometallic, *i.e.* all atoms in the NP are of the same chemical element. Bimetallic particles constitute yet another type of interesting systems for which abundant literature exists, from either theory or experiment, which is not reviewed here although we must mention that composition and order of elements can result in core@shell or amorphous particles, each type with its own particularities in structure and chemical reactivity. The atomic structure of isolated bimetallic NPs is nowadays a hot field, although theoretical studies concerning the reactivity of these systems are rather scarce.

Last but not least one must realize that metallic NPs as presented in this work are ideal entities, since these objects are usually found either covered by stabilizing agents or deposited on convenient supports. The reactivity of supported NPs is also a field in itself although still in its infancy. Again, for very large particles the effect of the support can be neglected and the chemistry is dominated by the exhibited surface sites. However, for small or medium particles, the support can be an active player and largely influence the chemistry. It is precisely in this type of systems where engineering at the molecular level is likely possible, and can play a decisive role. The last shown systems are clear examples that this chemistry is not only at hand but can be understood to design more active and efficient catalysts.

Acknowledgements

This work was supported by the Spanish MICINN and MINECO (FIS2008-02238 and CTQ2012-30751 grants, respectively) and by *Generalitat de Catalunya* (grants 2009SGR1041 and XRQTC). F.V. thanks the MINECO for a postdoctoral *Juan de la Cierva* grant (JCI-2010-06372), F.I. acknowledges additional support through the ICREA Academia award for excellence in research, and J.R.B.G. thanks *Fundação para a Ciência e a Tecnologia* (FCT), Lisbon, and the European Regional Development Fund (FEDER), within the frame of the COMPETE program for projects PTDC/QUI-QUI/117439/2010, FCOMP-01-0124-FEDER-020977, and PEst-C/CTM/LA0011/2013, and for *Programa Investigador* FCT.

References

1 M. A. El-Sayed, *Acc. Chem. Res.*, 2001, **34**, 257–264.
2 Catalytic Science Series, *Supported Metals in Catalysis*, ed. J. A. Anderson and M. Fernández-García, Imperial College Press, London, 2nd edn, 2011, vol. 11.
3 P. V. Kamat, *J. Phys. Chem. B*, 2002, **106**, 7729–7744.
4 Y. Xia, Y. Xiong, B. Lim and S. E. Skrabalak, *Angew. Chem., Int. Ed.*, 2009, **48**, 60–103.
5 H. M. Chen and R.-S. Liu, *J. Phys. Chem. C*, 2011, **115**, 3513–3527.
6 K. Saha, S. S. Agasti, C. Kim, X. N. Li and V. M. Rotello, *Chem. Rev.*, 2012, **112**, 2739–2779.
7 W. T. Yu, M. D. Porosoff and J. G. Chen, *Chem. Rev.*, 2012, **112**, 5780–5817.
8 M. Sterrer and H. J. Freund, *Catal. Lett.*, 2013, **143**, 375–385.
9 L. N. Lewis, *Chem. Rev.*, 1993, **93**, 2693–2730.
10 J. P. Wilcoxon and B. L. Abrams, *Chem. Soc. Rev.*, 2006, **35**, 1162–1194.
11 M. M. Kappes, *Chem. Rev.*, 1988, **88**, 369–389.
12 M. T. Reetz, W. Helbig, S. A. Quaiser, U. Stimming, N. Breuer and R. Vogel, *Science*, 1995, **267**, 367–369.
13 H. Lee, S. E. Habas, S. Kweskin, D. Butcher, G. A. Somorjai and P. D. Yang, *Angew. Chem., Int. Ed.*, 2006, **45**, 7824–7828.
14 G. A. Somorjai and J. Y. Park, *Chem. Soc. Rev.*, 2008, **37**, 2155–2162.
15 Y. Lu and W. Chen, *Chem. Soc. Rev.*, 2012, **41**, 3594–3623.
16 M. Turner, V. B. Golovko, O. P. H. Vaughan, P. Abdulkin, A. Berenguer-Murcia, M. S. Tikhov, B. F. G. Johnson and R. M. Lambert, *Nature*, 2008, **454**, 981–984.
17 F. Baletto and R. Ferrando, *Rev. Mod. Phys.*, 2005, **77**, 371–423.
18 R. Ferrando, J. Jellinek and R. L. Johnston, *Chem. Rev.*, 2008, **108**, 845–910.
19 I. V. Yudanov, R. Sahnoun, K. M. Neyman and N. Rösch, *J. Chem. Phys.*, 2002, **117**, 9887–9896.
20 K. Honkala, A. Hellman, I. N. Remediakis, A. Logadottir, A. Carlsson, S. Dahl, C. H. Christensen and J. K. Norskov, *Science*, 2005, **307**, 555–558.
21 O. D. Haberlen, S. C. Chung, M. Stener and N. Rosch, *J. Chem. Phys.*, 1997, **106**, 5189–5201.
22 F. Viñes, F. Illas and K. M. Neyman, *J. Phys. Chem. A*, 2008, **112**, 8911–8915.
23 A. Bruix, J. A. Rodriguez, P. J. Ramírez, S. D. Senanayake, J. Evans, J. B. Park, D. Stacchiola, P. Liu, J. Hrbek and F. Illas, *J. Am. Chem. Soc.*, 2012, **134**, 8968–8974.
24 S. T. Bromley, I. de P. R. Moreira, K. M. Neyman and F. Illas, *Chem. Soc. Rev.*, 2009, **28**, 2657–2670.
25 W. A. de Heer, *Rev. Mod. Phys.*, 1993, **65**, 611–673.
26 M. Boronat, A. Leyva-Pérez and A. Corma, *Acc. Chem. Res.*, 2013, DOI: 10.1021/ar400068w.

27 J. Sauer, *Chem. Rev.*, 1989, **89**, 1–199.
28 P. L. Hansen, J. B. Wagner, S. Helveg, J. R. Rostrup-Nielsen, B. S. Clausen and H. Topsoe, *Science*, 2002, **295**, 2053–2055.
29 M. C. Desjonqueres and D. Spanjaard, *Concepts in Surface Physics*, Springer-Verlag, Belin, 1996.
30 A. S. Barnard and P. Zapol, *J. Chem. Phys.*, 2004, **121**, 4276–4283.
31 G. Kresse and J. Furthmuller, *Phys. Rev. B: Condens. Matter Mater. Phys.*, 1996, **54**, 11169–11186.
32 C. Sousa, S. Tosoni and F. Illas, *Chem. Rev.*, 2013, **113**, 4456–4495.
33 C. J. Cramer and D. G. Truhlar, *Phys. Chem. Chem. Phys.*, 2009, **11**, 10757–10816.
34 I. V. Yudanov, R. Sahnoun, K. M. Neyman, N. Rösch, J. Hoffmann, S. Schauermann, V. Johánek, H. Unterhalt, G. Rupprechter, J. Libuda and H.-J. Freund, *J. Phys. Chem. B*, 2003, **107**, 255–264.
35 I. V. Yudanov, A. Genest, S. Schauermann, H.-J. Freund and N. Rösch, *Nano Lett.*, 2012, **12**, 2134–2139.
36 J. Kleis, J. Greeley, N. A. Romero, V. A. Morozov, H. Falsig, A. H. Larsen, J. Lu, J. J. Mortensen, M. Dułak, K. S. Thygesen, J. K. Nørskov and K. W. Jacobsen, *Catal. Lett.*, 2011, **141**, 1067–1071.
37 K. M. Neyman, C. Inntam, A. B. Gordienko, I. V. Yudanov and N. Rösch, *J. Chem. Phys.*, 2005, **122**, 174705.
38 F. Viñes, K. M. Neyman and A. Gorling, *J. Phys. Chem. A*, 2009, **113**, 11963–11973.
39 H. A. Aleksandrov, F. Viñes, W. Ludwig, S. Schauermann and K. M. Neyman, *Chem.–Eur. J.*, 2013, **19**, 1335–1345.
40 J. L. C. Fajín, A. Bruix, M. N. D. S. Cordeiro, J. R. B. Gomes and F. Illas, *J. Chem. Phys.*, 2012, **137**, 034701.
41 A. Roldán, J. M. Ricart and F. Illas, *Theor. Chem. Acc.*, 2011, **128**, 675–681.
42 P. S. West, R. L. Johnston, G. Barcaro and A. Fortunelli, *Eur. Phys. J. D*, 2013, **67**, 165.
43 W. Tang, L. Zhang and G. Henkelman, *J. Phys. Chem. Lett.*, 2011, **2**, 1328–1331.
44 W. An and P. Liu, *J. Phys. Chem.*, 2013, **117**, 16144–16149.
45 I. Y. Yudanov, A. V. Matveev, K. M. Neyman and N. Rösch, *J. Am. Chem. Soc.*, 2008, **130**, 9342–9352.
46 F. Viñes, C. Loschen, F. Illas and K. M. Neyman, *J. Catal.*, 2009, **266**, 59–63.
47 F. Viñes, Y. Lykhach, T. Staudt, M. P. A. Lorenz, C. Papp, H.-P. Steinrück, J. Libuda, K. M. Neyman and A. Görling, *Chem.–Eur. J.*, 2010, **16**, 6530–6539.
48 M. Haruta, *Nature*, 2005, **437**, 1098.
49 M. Boronat and A. Corma, *Dalton Trans.*, 2010, **39**, 8538–8546.
50 B. Cao, A. K. Starace, O. H. Judd, I. Bhattacharyya, M. F. Jarrold, J. M. López and A. Aguado, *J. Am. Chem. Soc.*, 2010, **132**, 12906–12918.